[CANCER RESEARCH 62, 5301–5307, September 15, 2002]

Fully Automated Three-Dimensional Tracking of Cancer Cells in Collagen Gels: Determination of Motility Phenotypes at the Cellular Level[1]

Zoe N. Demou and Larry V. McIntire[2]

Steele Laboratory for Tumor Biology, Department of Radiation Oncology, Massachusetts General Hospital/Harvard Medical School, Boston, Massachusetts 02114 [Z. N. D.], and Institute of Biosciences and Bioengineering, Cox Laboratory for Biomedical Engineering, Rice University, Houston, Texas 77005-1892 [L. V. M.]

ABSTRACT

We developed a fully automated three-dimensional cell tracking system that quantified the effect of extracellular matrix components on the infiltration and migration of tumor cells. The three-dimensional trajectories of two highly invasive cell lines, the human HT-1080 fibrosarcoma and the human MDA-MB-231 adenocarcinoma, were determined for long-term infiltration in plain or Matrigel-containing collagen type I gels. We modeled the trajectories with a novel formulation of the continuous Markov chain model that can distinguish between the tendencies for infiltration or lateral motion. Parameters such as the speed of subpopulations, the persistence of motion in certain directions, the turning frequency of the cells, the ultimate direction of motion, and the cell distribution with the infiltration depth were obtained to quantify the migration and infiltration at the cellular level. Distinct migratory and infiltration phenotypes were identified for the two cell types that were significantly dependent on gel composition. The HT-1080 cell line expressed a high motility phenotype on the plain collagen gel surface. The Matrigel-containing gel significantly enhanced the infiltration and the turning frequency of the HT-1080 cells. This study shows that tumor cell infiltration and migration are dynamic processes that depend significantly on the cell type and the microenvironment.

INTRODUCTION

Metastasis is not a random phenomenon but the result of complex biochemical and biophysical interactions because the ECM[3] functionally interacts with the metastasizing cells during most of the steps of the metastatic cascade (1).

A reliable *in vitro* model for quantifying the directional motion of cancer cells is critical for defining the mechanisms by which tumors invade *in situ* and for designing and evaluating antimetastatic therapies. There is significant evidence that tumors contain cell subpopulations with different malignant potential, growth rate, drug sensitivity, migration, or response to chemotactic factors (2). Results derived from the Boyden chamber, the most popular invasion assay, reflect the behavior of large cell populations (rather than single cells) and could be strongly biased by the relative proportion of the responding, or nonresponding cells in a heterogeneous population (3).

Infiltration of three-dimensional collagen gels provides a more realistic assay that may additionally involve different mechanisms, or different receptors compared with migration on two-dimensional slides, or in a Boyden chamber (4). A practical difficulty associated with the three-dimensional substrates for migration is the tedious determination of the cell positions in their bulk when performed manually. Only a few systems have been reported to track cells in three dimensions with relatively little manual involvement. These videomicroscopy-based cell tracking systems in three-dimensional gels were a significant improvement over the two-dimensional cell migration assays or the Boyden chamber (5–9).

Most of the *in vitro* cancer invasion data or cell tracking data in general has been modeled as a random walk, or it was analyzed to extract diffusion coefficients, persistence, or the average speed of the cell population. Although all these parameters have been successful in comparing the motility of cells, they have not provided a detailed characterization of the migration process. An adequate description of the cell locomotion requires parameters such as: (*a*) the population percentage of the motile cells; (*b*) the distribution of the cell population with the speed of locomotion; (*c*) the directionality of motion among the cell population; (*d*) the duration of motion in a certain direction; (*e*) the turning frequency of the cells; and (*f*) the preferred direction of motion in case of chemotaxis or spatial heterogeneities (10). The Markov chain model, as implemented for cell tracking, can provide such information and was a substantial innovation to the quantitative analysis of cell trajectories.

We developed a fully automated system for cell tracking in three dimensions and combined it with an innovative 13-state Markov chain to study the motility of two tumor cell types on different matrices. To the best of our knowledge, this is the first study of tumor cell infiltration in collagen gels that quantifies distinct directional motion at the cellular level associated with the microenvironment.

MATERIALS AND METHODS

Cell Culture. Two American Type Culture Collection cell lines, the human fibrosarcoma HT-1080 and the human breast adenocarcinoma MDA-MB-231, were cultured in DMEM with 10% fetal bovine serum, and 1% P/S. At approximately 90% cell confluence, the culture medium was removed, and the cells were incubated overnight in DMEM containing 0.5% fetal bovine serum and 1% P/S (infiltration medium). The cells were harvested with short exposure to EDTA, suspended in infiltration medium, and seeded on the top of the gels in a density of 3×10^3 cells/cm^2. The gels were placed in a humidified 5% CO_2 incubator until the tracking was initiated, 12 and 24 h after seeding for the HT-1080 and the MDA-MB-231, respectively. This lag period allowed for sufficient initiation of the cell infiltration.

Three-Dimensional Substrates. Plain collagen type I gels and alloy gels made of collagen type I and Matrigel were prepared by modifying the protocol of Faassen *et al.* (11). The collagen solutions were poured into polyethylene terepthalate cell culture inserts (Falcon, 8-μm pores) and placed into 6-well plates to form 2–3-mm thick gels. After 1 h of curing in a humidified CO_2 incubator, infiltration medium was placed on top of the gel and in the lower compartment to minimize nutrient and oxygen gradients. The collagen type I gels contained 61.7% v/v Vitrogen (Cohesion, Palo Alto, CA), 29% DMEM, 9.1% PBS, and 0.2% P/S. The alloy gels were a mixture of 57% v/v Vitrogen, 8% Matrigel (Collaborative Biomedical, Bedford, MA), 27% DMEM, 7.8% PBS, and 0.2% P/S. Vitrogen is a pepsin-solubilized bovine dermal collagen type I. Matrigel is a basement membrane extract from the Engelbreth-Holm-Swarm mouse sarcoma and contains laminin, collagen type IV, proteoglycans, entactin, nidogen, and growth factors that naturally occur in the Engelbreth-Holm-Swarm tumor such as transforming growth factor β, fibroblast growth factor, and tissue plasminogen activator.

In this paper, data are presented for HT-1080 fibrosarcoma cells in plain collagen type I gels and alloy gels and for MDA-MB-231 cells in alloy gels because the adenocarcinoma cells did not penetrate the plain collagen significantly even after 24 h.

Received 2/2/01; accepted 7/15/02.

The costs of publication of this article were defrayed in part by the payment of page charges. This article must therefore be hereby marked *advertisement* in accordance with 18 U.S.C. Section 1734 solely to indicate this fact.

[1] This work was supported by NIH Grant HL18670 and Robert A. Welch Foundation Grant C-938.

[2] To whom requests for reprints should be addressed, at Rice University, Institute of Biosciences & Bioengineering, MS-144, 6100 Main Street, Houston, TX 77005.

[3] The abbreviations used are: ECM, extracellular matrix; P/S, penicillin-streptomycin; MMP, matrix metalloproteinase.

Experimental Equipment. The videomicroscopy setup included: a Nikon Diaphot-inverted microscope and Hoffman Modulation Contrast Optics (Modulation Optics, Greenvale, NY); a custom made humidified microincubator that controlled the gel environment to 37°C and physiological pH; a computer-controlled microscope stage (Ludl Electronic Products Ltd, Hawthorne, NY) equipped with X, Y, and focus (Z) control modules; a Panasonic WV-BL200 video camera; and the FlashPoint 128 capture board (Integral Technologies, IN). The heart of the automated cell tracking system was an IBM Intellistation M Pro and the Optimas 6.2 image analysis software (Media Cybernetics L.P., Silver Spring, MD). The programs performing stage positioning, image acquisition, image analysis, cell identification, and trajectory reconstruction were written in the interpreter Analytical Language of Images supported by the Optimas software. Data analysis was a shared task between Analytical Language of Images and Matlab programs.

Image Acquisition. Three-dimensional images of the gels were acquired at $\times 10$ magnification with time lapse optical sectioning at adjacent XY fields of view forming a total field of 0.28 mm^2. The step for the optical sectioning or the distance between sequential Z fields was 20 μm.

Image Analysis. The image analysis was performed on the $\times 10$ raw images. A series of filter operations removed noise and enhanced the image features to prepare for thresholding whereby the outline of each cellular trace was defined. Then the positional coordinates (X, Y) of the area centroid (which defines the cell location) and the gray level in the outlined area were extracted.

Cell Identification and XYZ Extraction. Because of light scattering throughout the three-dimensional gel, traces of a certain cell exist at the Z sections both above and below its body limits so that multiple triplets (X, Y, gray level variation) of the image analysis data corresponded to the same cell. The role of the cell identification routine is to find the triplet that best represents an individual cell. The Z position of a cell was the Z section where the cellular trace had the maximum contrast.

Trajectory Reconstruction of Individual Cells. The trajectory reconstruction program assembled the (t, X, Y, Z) data, as acquired from the cell identification, in a time-ordered fashion to form the path of migration for each individual cell (*i.e.,* the cell trajectory). This program is a nearest neighbor algorithm modified to maintain the individuality of cells with crossing paths and to identify cells that move into or out of the three-dimensional tracking field. The major selection criterion is based on the fact that the translocation of a cell between two sequential time points is restricted to a maximum depending on the speed of locomotion. For example, if a cell moves 0.5 μm/min, its maximum possible translocation between two sequential time points t and $t + 30$ min is 15 μm (assuming constant speed). Therefore, the next position of the cell is the position of the closest neighbor among all of the cells identified within a distance less than the maximum possible translocation of the cell during this time lapse (according to the maximum speed of the cell population). The size of the nearest neighbor window depends on the cell speed and the time lapse for image acquisition, *i.e.,* the tracking efficiency of fast-moving cells would increase with more frequent image acquisition and a smaller nearest neighbor window.

To maximize the efficiency of the trajectory reconstruction during long-term tracking, phenomena such as cell proliferation, pathcrossing, and clustering were considered. During the tracking period, the number of tracked cells changes as cells divide, exit the tracking field, or as new cells, enter the field. If new cells (daughters or newcomers) appeared in the tracking field, they were identified as new individuals and tracked thereafter similarly to the old cells. For cells exiting the tracking field, the trajectories were terminated at the corresponding time point. When reentering the field, the cell trajectory was considered a continuation of the original cell trajectory if the reentry occurred within 3 time points from the time of exit and only if, when reentering, the cell met the nearest neighbor condition with the (X, Y, Z) last identified before the exit.

In the event of pathcrossing followed by cell separation (at the next time point), the program continued the trajectories reconstructed before the collision. In that case based only on the nearest neighbor criterion, an uncertainty for the exact cell identity may arise. Additional criteria taking into consideration morphological features such as cell size or orientation could be considered at this point but they also lead to uncertainties because of the highly dynamic morphology the cells assume during migration and especially during and after collisions. In such cases, it is often hard to determine the exact cell identity even for a user who tracks the cells visually from time lapse images (manual tracking).

When cells collided and proceeded as a cluster, which the image analysis routine successfully identified as multiple cells, the program continued to track the individual cells. In the case that the cluster was identified as a single cell, the trajectory of the cluster was the extension of one of the initial cell trajectories (that met the nearest neighbor criterion with respect to the cluster). On the other hand when the size of the cluster exceeded significantly the average cell size for 3 sequential time points, the trajectories leading to the particular cluster were terminated. Finally, in addition to these tracking techniques, the relatively low seeding density (3×10^3 cells/cm^2) decreased the probability for intercellular collisions, clustering, or pathcrossing, therefore increasing the tracking efficiency.

Obviously, appropriate definition of the experimental parameters determines the efficiency of the cell tracking technique. A cell population, even in the case of cell lines, includes subpopulations with different migratory characteristics. The experimental tracking parameters (*i.e.,* seeding density, total time of cell tracking, time lapse for image acquisition, size for cell identification, and trajectory reconstruction windows) depend significantly on these characteristics. For example, to follow a fast moving (sub)population, we would need lower cell seeding density, more frequent image acquisition, and relatively larger size windows for cell identification and trajectory reconstruction. Terminal restrictions, or experimental borders, may arise in this case, *i.e.,* the hard drive capacity for image saving (in case of off-line analysis), the lower limit in the time lapse for image acquisition, which cannot be smaller than the time required for the motion of the motorized stage during the image acquisition, or smaller than the duration of image analysis (execution time for image analysis routine) for on-line image analysis.

Data Analysis. Three separate sets of experiments have been performed for each cell line on each matrix, and the one-way ANOVA was performed to test the significance of the data. $P < 0.05$ was considered significant. The data are presented and plotted as average $\pm$ SD.

The tracking program extracts the four-dimensional position vector [t, X, Y, Z] (Fig. 1) of all of the cells that existed in the three-dimensional tracking field during the tracking period. Only cells residing the tracking field for 95% of the total time were fed to the data analysis program because the goal was to study long-term behavior of the cells. An average of 60 HT-1080 and 80 MDA-MB-231 cells tracked/three-dimensional field met this criterion. The efficiency of the automated tracking increased with lower cell motility and seeding density and reached a maximum of 93% compared with the manual approach. To perform this comparison, we created composite digital images by overlapping the cell identification number 1 to $N(t)$ [*i.e.,* "1" for cell 1, "2" for cell 2, etc., and $N(t)$ is the total number of cells identified at time point t] to the images acquired via time lapse optical sectioning. Then by displaying the composite images sequentially (*i.e.,* in a form of a time lapse movie), the user can determine whether the automatically tracked trajectory, as formed by the sequential positions of each cell identification number on the digital monitor, coincides with the actual trajectory of a particular cell.

The following parameters were used to analyze the cell trajectories.

Average Speed of Cell Locomotion. The average speed of all of the individual cells was calculated considering only the time points when the cell was in motion (displacements larger than the average half-cell diameter):

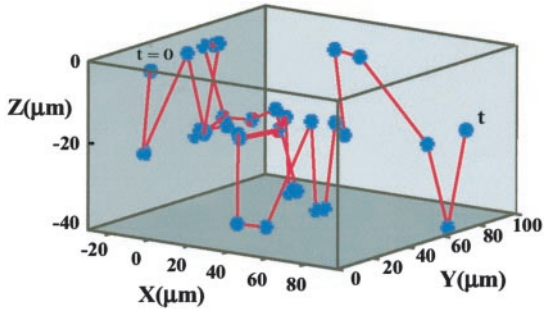

Fig. 1. Typical trajectory of a tracked HT-1080 fibrosarcoma cell during 16 h in a collagen type I gel. The *points* represent the sequential positions of the cell centroid every 30 min as extracted from the cell tracking program throughout the tracking period.

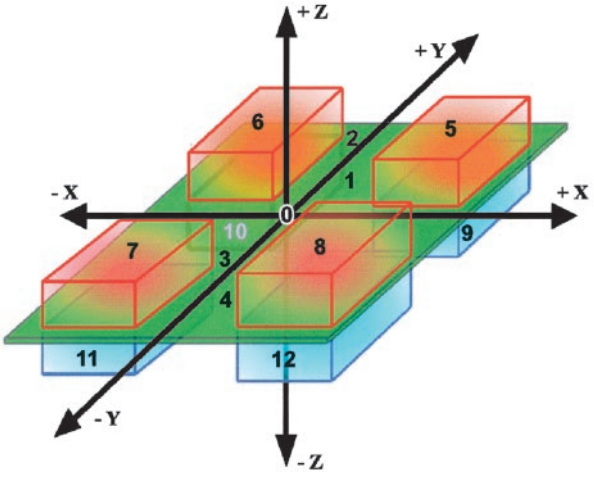

Fig. 2. The 13 states of the Continuous Markov Chain Model. The Cartesian three-dimensional space is divided into 13 subspaces (states). Each possible direction of motion is mapped to 1 of the 12 directional subspaces. States 1–4 represent cells moving in the XY plane (parallel to the gel-medium interface). States 5–8 describe cells moving toward the top of the gel (positive Z direction), and states 9–12 represent cells infiltrating the gel (negative Z direction). For example, a cell is at state 1 if it moves on the Z = 0 plane in positive X and positive Y direction. Similarly, a cell is at state 12 if it is infiltrating the gel (negative Z direction) heading in a positive X and negative Y direction. Cells at state 0 (stationary state) move less than half-cell diameter between two successive time points.

$$\bar{V}_i = \frac{\sum_{t=1}^{N} d_i(t)}{N\Delta t} \qquad \text{(a)}$$

$d_i(t)$ is the cell displacement of the cell i between time t and the previous time point (t-1), Δt is the time lapse for image acquisition, and N is the number of times that the cell has a nonzero displacement during the tracking period.

Continuous Markov Chain Model. The continuous Markov model can quantify migration in three dimensions at the cellular level (5, 10, 12). This model divides the Cartesian space into subsets namely the Markov states. According to the Markov theory, the trajectory of each cell is described as a stochastic process so that the direction of motion between successive time points is mapped to one of the Markov states. We expanded the Noble and Levine approach (12) by defining a novel Markov chain with 12 directional and 1 stationary state to distinguish between lateral (XY) and vertical (Z) motion during gel infiltration (Fig. 2). The direction of motion of a cell is calculated from the positional differences Δx, Δy, and Δz between successive time points, and then the appropriate Markov state is assigned to a cell. Nonzero displacements must be larger than half-cell diameter. The cell migration parameters from the Markov model are the:

(*a*) Waiting times (T_i), which give the average time that cells spend at each state, or the persistence of motion in a certain direction. The expected value of the waiting time at state i is:

$$E(T_i) = \frac{\text{(total time that all cells spent in state } i\text{)}}{\text{(total number of transitions out of state } i\text{)}} \qquad \text{(b)}$$

(*b*) Transition probabilities ($p(i/j)$), which give the probability of a cell currently at state j to transit to state i, where $j \neq i$. These probabilities quantify the changes in the direction of motion and, thus, the turning behavior of the cells.

$$p(i/j) = \frac{\text{(number of transitions from state } j \text{ to state } i\text{)}}{\text{(number of transitions from state } j \text{ to any other state)}} \qquad \text{(c)}$$

(*c*) Steady-state probabilities, which define the ultimate probability of motion as time goes to infinity. Waiting times and transition probabilities were directly calculated from the measured cell trajectories, whereas steady-state probabilities are predicted from the statistical model. These probabilities are the solution of a homogeneous system of equations with order being the number of states (*i.e.,* 13 steady-state probabilities are predicted for the 13 state Markov model). Disproportionately high values of some steady-state probabilities indicate an ultimate preference for a certain direction.

RESULTS

The data analysis revealed distinct motility phenotypes in the two cell lines and gel types characterized by significantly different patterns for the parameters studied.

Speed of Cell Locomotion. Fig. 3*a* shows the average cell speed of each HT-1080 cell tracked in alloy gel in a typical experiment. To summarize cell speed in all experiments, we plotted the distribution of the cell populations according to their average speed using grouped speed ranges (Fig. 3*b*). There was no significant difference in the distribution of fibrosarcoma cells on either matrix, although the overall average speed increased from 0.6 ± 0.07 μm/min in collagen type I gels to 0.7 ± 0.06 μm/min in alloy gels ($P = 0.11$). The subpopulations at the lower speed range of <0.5 μm/min were similar for both cell lines and matrices and constituted ~37% of the total cell population. However, the subpopulations at the higher speeds were characteristic of the tumor cell type with large number of the fibrosarcoma cells both in collagen I (38.0 ± 4.3%) and in alloy (46.6 ± 9.1%), maintaining speeds higher than 0.7 μm/min, whereas only 24.8 ± 2.9% of the adenocarcinoma cells reached this speed level.

Waiting Times. Fig. 4 shows that the average waiting time in the stationary state for fibrosarcoma cells in collagen type I gels was 34.3 ± 2.0 min and similar to the average duration of lateral motion

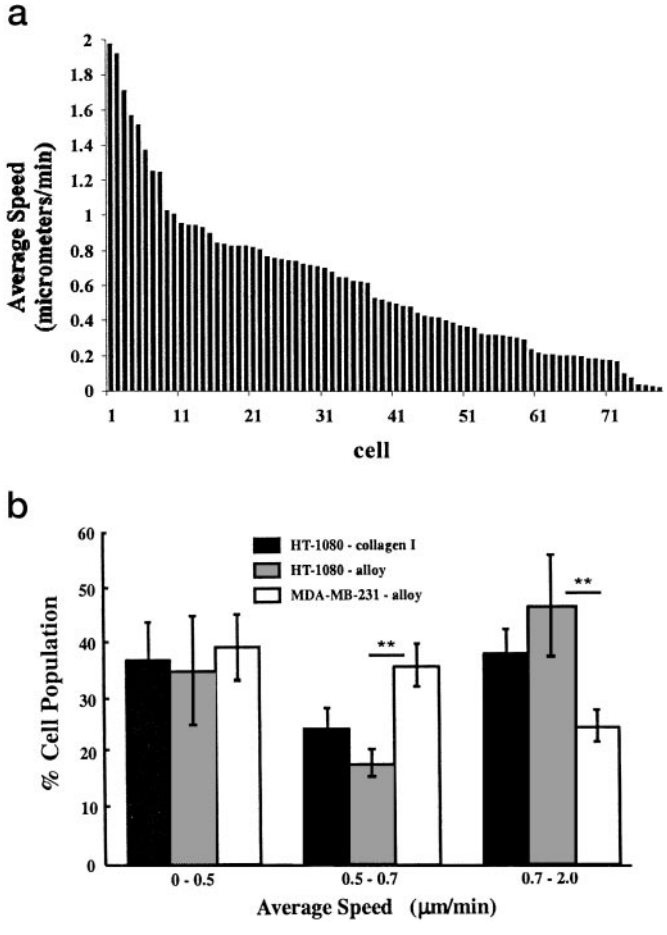

Fig. 3. *a*, average speed values for all of the HT-1080 cells for a typical tracking experiment in alloy gel. *b*, distribution of the cell population according to the average speed of cell locomotion for HT-1080 ($n = 3$) on collagen type I gels, HT-1080 ($n = 3$) on alloy (Collagen I - Matrigel) gels, and MDA-MB-231 ($n = 3$) on alloy gels. The *error bars* show the computed SD. The *asterisks* indicate significant differences.

(states 1–4), 34.9 ± 3.1 min. In collagen I, the persistence of fibrosarcoma cells in the stationary state and the lateral motion states was significantly 5–10 min longer than the average duration of upwards migration (Z+ motion), 26.6 ± 0.4 min (states 5–8) or downward migration (Z− motion), 27.1 ± 0.6 min (states 9–12).

The HT-1080 cells in the alloy decreased both their persistence in the stationary state (29.7 ± 4.4 min) and their persistence in lateral motion (31.4 ± 1.6 min) compared with these cells in collagen I gels, but no significant change occurred in the duration of migration up (Z+), 26.8 ± 1.4 min or migration down (Z−), 27.5 ± 1.3 min. However, in the alloy, the reduced stationary time and unchanged duration of Z motion eliminated the differences observed in collagen I, whereas the lateral motion was still significantly longer.

The waiting times of the MDA-MB-231 cells on alloy gels followed a totally different trend showing significantly lower motility. Their stationary time of 55.9 ± 7.5 min was dramatically 30–35 min longer than the average duration of planar motion (23.7 ± 1.0 min), migration up (21.6 ± 0.8 min) or down (21.6 ± 0.9 min), whereas the lateral and Z motion (up or down) were comparable. The stationary time of the MDA-MB-231 cells was significantly about 20 min longer than the stationary time of the HT-1080 cells, whereas in contrast to the HT-1080, there was no preference for any of the directional states because the planar motion of the MDA-MB-231 cells was only slightly ($P = 0.08$) longer than the Z motion.

Transition Probabilities. Fig. 5 gives the transition probabilities for HT-1080 cells on alloy gels. The HT-1080 cells in alloy are shown because their transitions were more frequent. The transition profiles of HT-1080 cells in collagen I gels are less dramatic; for the adenocarcinoma cells, the profiles were even smoother, revealing little turning activity. For clarification, we plotted transitions among groups of geometrically equivalent states (Fig. 6). These states are: the stationary state (state 0); the state of lateral motion (states 1–4); the state of Z+ motion (states 5–8); and the state of Z− motion (states 9–12).

Fibrosarcoma cells on collagen type I (Fig. 6*a*) had a high probability of shifting into and maintaining lateral motion. Stationary cells had a higher probability (54.0 ± 4.9%) of entering a state of planar motion rather than moving up (25.2 ± 2.2%) or down (20.8 ± 2.6%; $P \ll 0.01$). When transitions from the plane to Z occurred, the Z− directions were slightly more probable ($P = 0.15$). The continuation of lateral motion (36.5 ± 1.5%) was significantly more probable than stopping (27.5 ± 0.7%), whereas a Z motion was quite unlikely. However, when entering a Z motion, laterally moving cells had a significantly higher probability for Z− (20.8 ± 1.7%) because the majority of laterally moving cells existed on the top of the gel. The transitions from the Z+ and Z− states were of great interest. Infiltrating (Z−) cells had a strikingly high probability to transit into a Z+ state of motion and *vice versa*. The next most favorable transition from the Z motion states was to the states of planar motion (~30%). Overall, invading

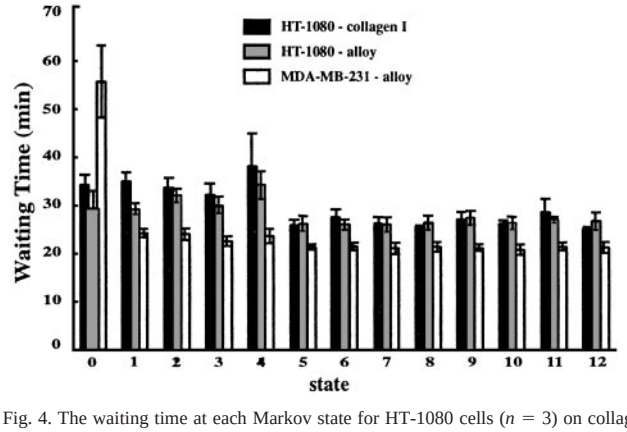

Fig. 4. The waiting time at each Markov state for HT-1080 cells ($n = 3$) on collagen type I gels, HT-1080 cells ($n = 3$) on alloy (Collagen I - Matrigel) gels, and MDA-MB-231 cells ($n = 3$) on alloy gels. The *error bars* represent the calculated SD.

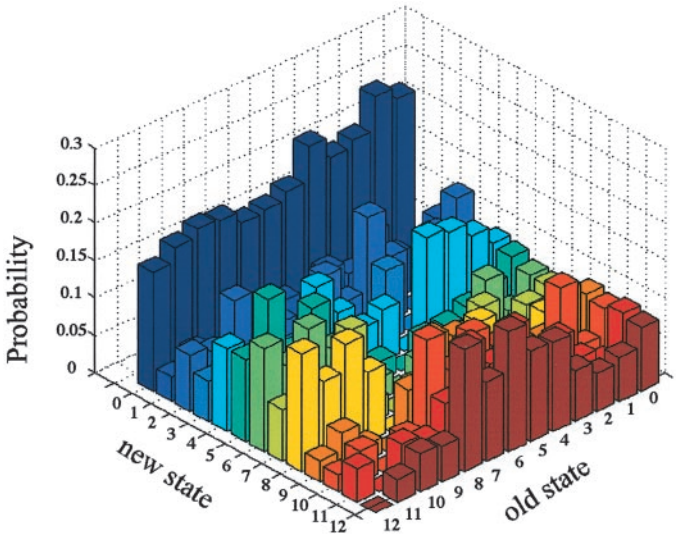

Fig. 5. Average transition probabilities ($n = 3$) for HT-1080 cells in alloy gels among the 13 Markov states.

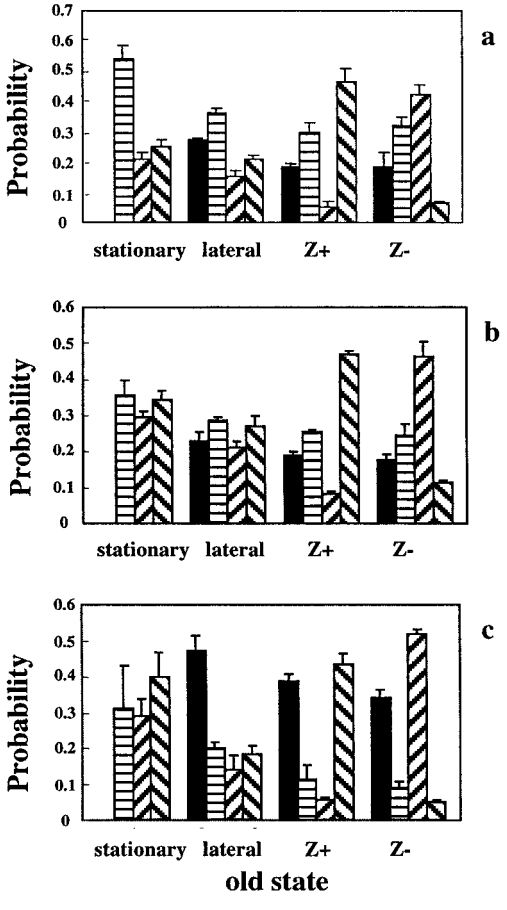

Fig. 6. Cumulative transition probabilities for HT1080 on collagen I gels (*a*), for HT1080 on alloy gels (*b*), and for MDA-MB-231 on alloy gels (*c*). Transitions are considered out of the stationary state, the lateral motion state (includes states 1–4 of XY motion), the Z+ motion state (includes states 5–8), and the Z− motion state (includes states 9–12). The new states are shown with (■) for the stationary state, (▤) for the lateral motion, (▨) the Z+ motion, and (▧) the Z− motion.

cells had a significantly smaller probability (~19%) to stop and 81% probability to maintain a state of motion.

In HT-1080 cells in alloy (Fig. 6*b*) there was a significant 35% decrease in the probability of stationary cells to shift into lateral motion compared with HT-1080 cells in plain collagen, accompanied with a significant 39.1% increase in the probability to move deeper in the gel (34.6 ± 2.8%) and a 44.2% increase in the probability for moving up (29.6 ± 2.2%). Infiltrating deeper in the gel was still the most probable direction of Z motion. Additionally, Matrigel significantly increased, an additional 30.2%, the probability of planar cells to move deeper in the gel (27.1 ± 3.5%) and a 40.4% increase for the opposite Z+ direction (21.3 ± 2.0%). Despite that, the planarly moving fibrosarcoma cells had 21% lower probability to maintain their two-dimensional motion (28.7 ± 1.0%) compared with cells in the plain collagen, and this motion was still more probable than shifting into the stationary (22.9 ± 3.2%) or the Z+ states. The oscillatory Z+ to Z− transition pattern was still well represented.

Although HT-1080 cells maintained a state of motion, in contrast, the MDA-MB-231 had high probabilities for immobility (Fig. 6*c*). Stationary adenocarcinoma cells showed no preference for any of the directional states. Transition to the Z− states had insignificantly higher probability (39.8 ± 8.8%) than the Z+ (29.1 ± 5.8%) or planar states (30.9 ± 14.5%). Laterally moving cells had a strikingly high probability of becoming stationary (47.2 ± 5.0%), whereas the probabilities for adopting planar or Z motions were similar. The motion of adenocarcinoma cells deviated partially from the oscillatory Z+, Z− transitions. Infiltrating Z− adenocarcinoma cells preferably shifted to Z+ direction of motion (51.9 ± 1.9%), whereas transitions to the stationary state were also quite probable (34.1 ± 3.0%). The transitions from Z+ to Z− states (43.7 ± 3.4%) were not as preferred as for the fibrosarcoma cells because transitions to immobility were also probable (39.0 ± 1.6%; $P = 0.097$).

Steady-State Probabilities. The stationary (or the motile) subpopulation and the potentials for lateral and Z motion were very distinctive among the cell and gel types, yet a common feature was the similar probabilities for the X, Y directional states (Fig. 7, states 1–4). We sum up the probabilities related to groups of geometrically equivalent Markov states (Fig. 8). Fibrosarcoma cells tended to be highly motile with a subpopulation of 79.6 ± 0.5% in motion in collagen I gels. The majority (52.7%) of the motile fibrosarcoma population was involved in planar motion (41.9 ± 0.7% of the total population in states 1–4), a significantly smaller percentage 21.8% was in Z+ (states 5–8) and in Z− motion (states 9–12), 25.5% of the motile population (17.4 ± 0.4% and 20.3 ± 0.2%, respectively, of the total

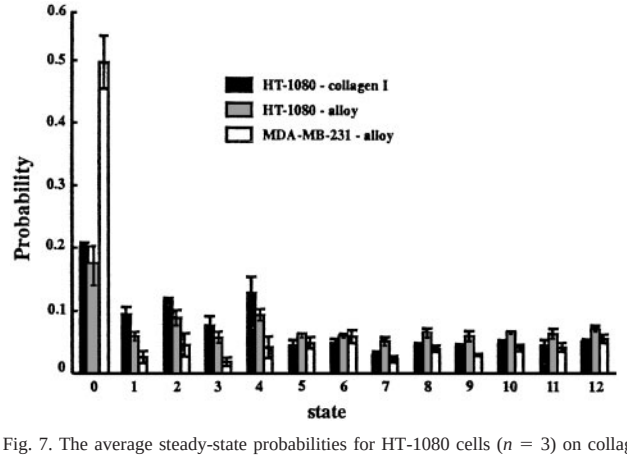

Fig. 7. The average steady-state probabilities for HT-1080 cells ($n = 3$) on collagen type I gels, HT-1080 cells ($n = 3$) on alloy (Collagen I - Matrigel) gels, and MDA-MB-231 cells ($n = 3$) on alloy gels. The *error bars* show the calculated SD.

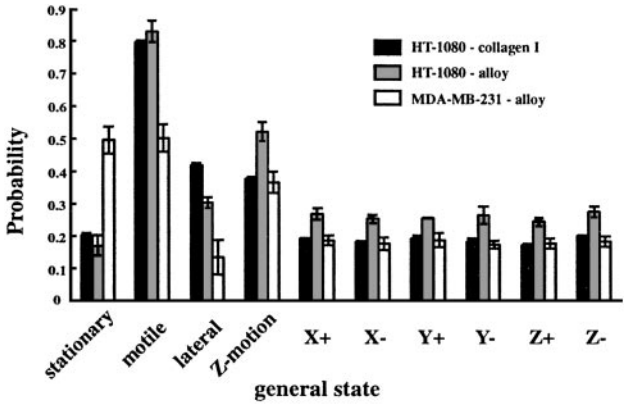

Fig. 8. Cumulative steady-state probabilities for HT-1080 cells ($n = 3$) on collagen type I gels, HT-1080 cells ($n = 3$) on alloy (Collagen I - Matrigel) gels, and MDA-MB-231 cells ($n = 3$) on alloy gels. The *error bars* show the calculated SD.

population). The Z− motion was significantly (16.7%) more probable than the Z+ motion.

Matrigel altered the preference of fibrosarcoma cells for planar motion, resulting in similar probabilities for planar and Z motions. It increased the motile fibrosarcoma subpopulation to 82.9 ± 3.2% but not significantly compared with the motility in plain collagen. However, the alloy gel resulted in a significant enhancement in Z transitions, shifting the fibrosarcoma cells from lateral to Z motion. The planar subpopulation on collagen type I decreased significantly to 30.4 ± 1.6% on alloy gels with parallel significant increase in the probability for Z motion to 52.4 ± 2.8% ($P < 0.01$).

The behavior of MDA-MB-231 cells on alloy gels was quite different. The adenocarcinoma cells had a much smaller motile subpopulation (50.3 ± 4.3%) that was preferentially engaged in a Z motion (36.6 ± 3.3%) rather than lateral motion (13.7 ± 5.4%). As in the case of fibrosarcoma cells in alloy gels, the steady-state probabilities for Z+ and Z− motion were similar. Quite interestingly, this Z motion potential of about 18% was comparable between the fibrosarcoma cells in plain collagen and the adenocarcinoma cells in alloy.

Infiltration Depth Over Time. Fig. 9 shows the invasion profiles of HT-1080 cells and MDA-MB-231 cells in the alloy gels. The Z distribution for the HT-1080 cells over time in both collagen I and alloy gels had similar trends. Both cases reflected advanced infiltration of the three-dimensional matrix and high transition frequency among the Z sections. About 90% of the initially seeded fibrosarcoma cells infiltrated the alloy gels, whereas only 75% invaded the plain collagen gels. The profile of fibrosarcoma cells on plain collagen I reached a maximum depth of 150 μm as opposed to 260 μm in alloy during the same tracking period. Adenocarcinoma cells invaded the alloy matrix significantly less. Only 70% of the initial cells left the gel surface, whereas >50% were located ~20–40 μm from the top of the gel. The invasion front was about 120 μm 59 h (24 + 35) after seeding, less than half of the front of fibrosarcoma cells in alloy, but 12 h later.

DISCUSSION

We present the first study that quantifies the directional locomotion of cells during gel infiltration as a set of time-dependent variables and at the cellular level. This work was built on two main foundations: a computer-based system for automated cell tracking in three dimensions, and a statistical analysis of the individual cell trajectories that computed distinct directional motility patterns associated with certain tumor cell lines and the gel composition.

Cancer invasion during metastasis has been characterized as a

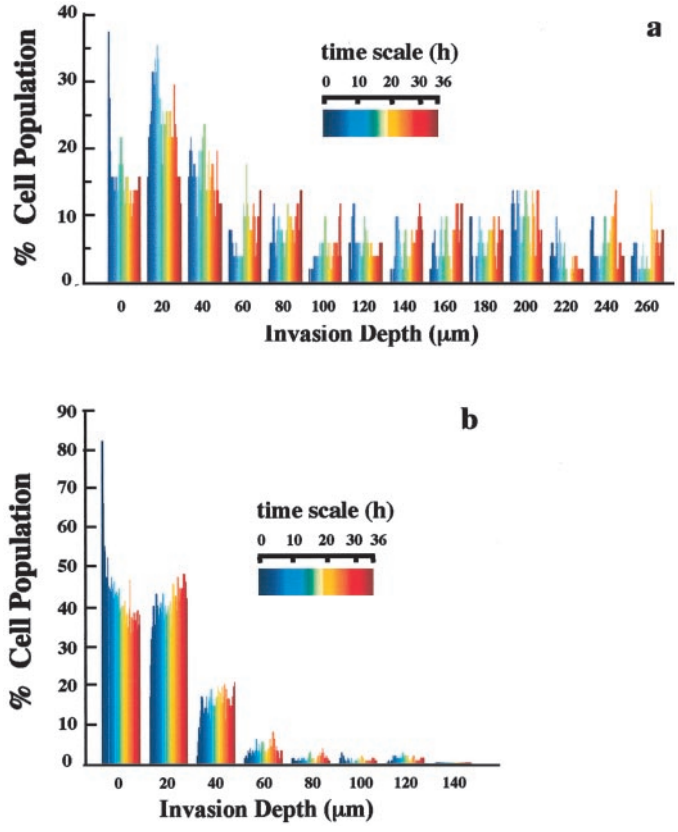

Fig. 9. *a*, distribution of the HT-1080 cell population with the depth of invasion in alloy gels over time. *b*, distribution of the MDA-MB-231 cell population with the depth of invasion in alloy gels over time. The data represent 36 h automated cell tracking that started 12 h after seeding for the HT-1080 cells (*a*) and 24 h after seeding for the MDA-MB-231 cells (*b*).

temporary phenomenon in which tumor cells are not continuously invasive but rather express an unstable phenotype depending on the stimuli generated from the surroundings (13, 14). It is possible that different groups of cells within a population respond differently to various biochemical and biophysical stimuli. These observations emphasize the need for an experimental model that follows the cancer invasion or the cell migration in general, as a dynamic and multifaceted action of individual cells, in which the characteristics evolve over time and throughout the three-dimensional tissue microenvironment.

The infiltration of collagen I gels by tumor cells was used as a model for stromal invasion during metastasis. A denser ECM is more representative of the natural tissue the tumor cells encounter. However, very dense gels (>2 mg/ml) reduce the light transmission in an optical system. Pure Matrigel layers have low density and lack mechanical integrity that may permit passive penetration rather than active cell-gel interaction (15). Thus Matrigel was mixed with collagen I to form thick gel structures of relatively high density that allowed evaluation of basement membrane components on infiltration and migration.

The continuous Markov chain model is a probabilistic approach that can describe the cell migration at the cellular level. Multiple migratory phenotypes were identified among the cell populations and quantified as probabilities of subpopulations. These subpopulations were defined by the Markov states, which for the three-dimensional migration, are subsets of the three-dimensional Cartesian space. We introduced a novel Markov chain with 13 states for the statistical analysis of the three-dimensional trajectories of the individual cells. Our model was able to identify cells moving laterally during gel infiltration as well as stationary and Z moving cells.

Matrigel did not alter significantly the kinetic characteristics of fibrosarcoma such as the motile subpopulation, the speed distribution, or the average speed of locomotion. However, it amplified the turning frequency and extent of infiltration by shifting a significant cell percentage from planar to Z− motion and reducing the persistence of fibrosarcoma cells for lateral motion. However, the motile subpopulation was a distinct characteristic of the cell type. HT-1080 cells in either matrix showed a significantly more motile behavior with larger motile subpopulation and higher average speed than MDA-MB-231 cells. In the alloy, ~50% of the HT-1080 cell population attained speeds of 0.7–2 μm/min, whereas >70% of MDA-MB-231 cells obtained speeds <0.7 μm/min (Fig. 3*b*). For both gel and cell types, the directional motion (X±, Y±, Z±) was random. The average speeds from our experiments (0.6–0.7 μm/min) are comparable with values found for other tumor cells in collagen gels, *e.g.*, 0.82 μm/min for mouse melanoma in Vitrogen gels (16) or 0.1 μm/min for MDA-MB-361 in collagen gels (Ref. 17; the 361 is a nontumorigenic and nonmetastatic member of the MDA breast adenocarcinoma cell lines).

The transition probabilities revealed that the HT-1080 cells preferred to maintain a state of motion. The directionality of their motion however, was dictated by the composition of their environment. In plain collagen gels, the majority of fibrosarcoma cells moved laterally whereas in alloy gels, they dramatically expanded their motion into the third dimension. In contrast, the MDA-MB-231 cells persisted in the stationary state for twice as long as they moved directionally. When moving, they were more likely to move vertically, but their duration of motion was short and often interrupted by long inert periods. There was a consistent pattern of significantly preferred transitions between Z+ and Z− for both cell and gel types. For HT-1080 cells in alloy gels, ~20% of the transitions from a Z motion state (*i.e.*, nonstationary and nonplanar) occurred in the exactly opposite Markov direction (*e.g.*, from state 8 to 10). The exactly opposite transitions, *i.e.*, from (−, +, −) to (+,−, +), were ~50% of all of the transitions from Z (states 5–12) to −Z (states 9–12). This behavior suggests that cells degrade their immediate surroundings and invade their way in the gel via an oscillatory motion in the path of least resistance. HT-1080 cells are known to leave well-defined tracks (depressions or channels) when migrating (18). A similar pattern was observed with Markov analysis for transformed 3T3 cells in collagen gels (5).

Fibrosarcoma cells infiltrated the alloy more than plain collagen but infiltrated both gels more efficiently than adenocarcinoma cells. The HT-1080 cell infiltration was faster and denser giving more cells/gel unit volume and formed a secondary peak in the infiltration profile (Fig. 9*a*) characteristic of their high motility and high transition frequency among the Z sections. The Z location and the cell concentration at the secondary peak depend on time and the matrix composition. The exponentially decreasing profile of adenocarcinoma cells (Fig. 9*b*) results from their low transition frequency and low motility. This pattern also represents initial stages of gel infiltration and could represent the infiltration profile of fibrosarcoma cells shortly after seeding (data not shown). The staggered motility of adenocarcinoma cells gave their infiltration a localized character in which cells had low tendency for lateral motion and infiltrated slowly into the immediately surrounding gel. The selection of the lag time preceding the tracking of the HT-1080 and MDA-MB-231 cells (12 and 24 h, respectively), was based on these infiltration profiles. It takes ~24 h for about 10% of the MDA-MB-231 cells to invade >20 μm inside the gel matrix. A lag of 12 h allows ~50% of the HT-1080 cells to be at least 40 μm inside the gel when tracking begins. Tracking of HT-1080 cells under these conditions was selected to show advanced infiltration of the matrix, whereas the MDA-MB-231 cells, showing a less aggressive infiltration, exemplify the initial stage of infiltration.

The HT-1080 and MDA-MB-231 cells produce similar MMPs. HT-1080 cells secrete MMP-9 and partially activate the endogenous MMP-2 proenzyme (19). The MDA-MB-231 cells express MMP-2 activator MMP-9 and show activated MMP-2 when cultured on Vitrogen, similarly to human fibroblasts (20). MMP-2 (gelatinase A) and MMP-9 (gelatinase B) are closely related and degrade specifically the gelatins from collagen type IV and V (21). In addition to the MMPs, HT-1080 cells secrete urokinase-type plasminogen activator, scatter factor, and an autocrine motility factor, which are important mediators of cell invasion and metastasis (22–24).

Higher proteolytic action combined with motility factors might explain the more active migration and robust infiltration of HT-1080 cells compared with MDA-MB-231 cells. The effect of Matrigel may be attributed, in part, to the collagen type IV content that would make the alloy gel more susceptible to degradation by fibrosarcoma-secreted gelatinases. Additionally, Matrigel contains several ECM components and growth factors that might have induced chemokinesis of the fibrosarcoma cells or activation of tumor-secreted enzymes that would ultimately enhance the enzymatic proteolysis of the gel and facilitated cell migration in the three-dimensional matrix.

The extracellular microenvironment influences the migratory phenotype expressed in three-dimensional matrices. We quantitated changes in speed, duration, turning frequency, and directionality of cellular motion. Our automated three-dimensional tracking combined with the Markov analysis provides a technique for the quantitative assessment of the migratory phenotype at the cellular level. This can be used to elucidate how ECM components modulate the characteristics of tumor invasion and quantify the effect of motility enhancing or inhibitory factors.

ACKNOWLEDGMENTS

We thank Dr. Suzanne G. Eskin for critical review of this manuscript.

REFERENCES

1. Mareel, M. M., De Baetselier, P., and Van Roy, F. M. Mechanisms of Invasion and Metastasis, pp. 98–99. Boca Raton: CRC Press, Inc., 1991.
2. Fidler, I. J., and Hart, I. R. Biological diversity in metastatic neoplasms: origins and implications. Science (Wash. DC), *217:* 998–1003, 1982.
3. Oda, D., and Orr, F. W. Effects of passage, growth phase, and heterogeneity of a tumor cell population on tumor cell chemotaxis. Invasion Metastasis, *4:* 189–197, 1984.
4. Schor, S. L. Cell proliferation and migration on collagen substrata *in vitro*. J. Cell Sci., *41:* 159–175, 1980.
5. Noble, P. B. Extracellular matrix and cell migration: locomotory characteristics of MOS-11 cells within a three-dimensional hydrated collagen lattice. J. Cell Sci., *87:* 241–248, 1987.
6. Vakaet, L., Jr., Vleminckx, K., Van Roy, F., and Mareel, M. Numerical evaluation of the invasion of closely related cell lines into collagen type I gels. Invasion Metastasis, *11:* 249–260, 1991.
7. Friedl, P., Noble, P. B., and Zanker, K. S. Lymphocyte locomotion in three-dimensional collagen gels. Comparison of three quantitative methods for analysing cell trajectories. J. Immunol. Methods, *165:* 157–165, 1993.
8. Dickinson, R. B., McCarthy, J. B., and Tranquillo, R. T. Quantitative characterization of cell invasion *in vitro*: formulation and validation of a mathematical model of the collagen gel invasion assay. Ann. Biomed. Eng., *21:* 679–697, 1993.
9. Awasthi, V., Doolittle, K. W., Parulkar, G., and McNally, J. G. Cell tracking using a distributed algorithm for three-dimensional-image segmentation. Bioimaging, *2:* 98–112, 1994.
10. Lee, Y., Markenscoff, P. A., McIntire, L. V., and Zygourakis, K. Characterization of endothelial cell locomotion using a Markov chain model. Biochem. Cell Biol., *73:* 461–472, 1995.
11. Faassen, A. E., Schrager, J. A., Klein, D. J., Oegema, T. R., Couchman, J. R., and McCarthy, J. B. A cell surface chondroitin sulfate proteoglycan, immunologically related to CD44, is involved in type I collagen-mediated melanoma cell motility and invasion. J. Cell Biol., *116:* 521–531, 1992.
12. Noble, P. B., and Levine, M. D. Computer-assisted Analysis of Cell Locomotion and Chemotaxis, pp. 125–131. Boca Raton: CRC Press, 1986.
13. Mareel, M. M., Van Roy, F. M., and Bracke, M. E. How and when do tumor cells metastasize? Crit. Rev. Oncog., *4:* 559–594, 1993.
14. Le Marer, N., and Bruyneel, E. Comparison of *in vitro* invasiveness of human breast carcinoma in early or late stage with their malignancy *in vivo*. Anticancer Res., *16:* 2767–2772, 1996.
15. Sieuwerts, A. M., Klijn, J. G., and Foekens, J. A. Assessment of the invasive potential of human gynecological tumor cell lines with the *in vitro* Boyden chamber assay: influences of the ability of cells to migrate through the filter membrane. Clin. Exp. Metastasis, *15:* 53–62, 1997.
16. Burgess, B. T., Myles, J. L., and Dickinson, R. B. Quantitative analysis of adhesion-mediated cell migration in three-dimensional gels of RGD-grafted collagen. Ann. Biomed. Eng., *28:* 110–118, 2000.
17. Niggemann, B., Maaser, K., Lu, H., Kroczek, R., Zanker, K. S., and Friedl, P. Locomotory phenotypes of human tumor cell lines and T lymphocytes in a three-dimensional collagen lattice. Cancer Lett., *118:* 173–180, 1997.
18. Kramer, R. H., Bensch, K. G., and Wong, J. Invasion of reconstituted basement membrane matrix by metastatic human tumor cells. Cancer Res., *46:* 1980–1989, 1986.
19. Deryugina, E. I., Luo, G. X., Reisfeld, R. A., Bourdon, M. A., and Strongin, A. Tumor cell invasion through matrigel is regulated by activated matrix metalloproteinase-2. Anticancer Res., *17:* 3201–3210, 1997.
20. Azzam, H. S., Arand, G., Lippman, M. E., and Thompson, E. W. Association of MMP-2 activation potential with metastatic progression in human breast cancer cell lines independent of MMP-2 production. J. Natl. Cancer Inst. (Bethesda), *85:* 1758–1764, 1993.
21. Mackay, A. R., Hartzler, J. L., Pelina, M. D., and Thorgeirsson, U. P. Studies on the ability of 65-kDa and 92-kDa tumor cell gelatinases to degrade type IV collagen. J. Biol. Chem., *265:* 21929–21934, 1990.
22. Watanabe, H., Carmi, P., Hogan, V., Raz, T., Silletti, S., Nabi, I. R., and Raz, A. Purification of human tumor cell autocrine motility factor and molecular cloning of its receptor. J. Biol. Chem., *266:* 13442–13448, 1991.
23. Park, W. S., Oh, R. R., Kim, Y. S., Park, J. Y., Shin, M. S., Lee, H. K., Lee, S. H., Yoo, N. J., and Lee, J. Y. Absence of mutations in the kinase domain of the Met gene and frequent expression of Met and HGF/SF protein in primary gastric carcinomas. APMIS, *108:* 195–200, 2000.
24. Webb, D. J., Nguyen, D. H., and Gonias, S. L. Extracellular signal-regulated kinase functions in the urokinase receptor-dependent pathway by which neutralization of low density lipoprotein receptor-related protein promotes fibrosarcoma cell migration and matrigel invasion. J. Cell Sci., *113:* 123–134, 2000.